Convolutional Neural Network for Ladder-Secondary Linear Induction Motor Fault Diagnosis

Malihe Heidary[1], Email: m.heidary@sru.ac.ir, Tel:+98-912-5306218,

Vahab Nekoukar[1], Email: v.nekoukar@sru.ac.ir, Tel:+98-912-5655331,

Peyman Naderi[1,*], Email: p.naderi@sru.ac.ir, Tel:+98-912-806-5207,

Abbas Shiri[1], Email: abbas.shiri@sru.ac.ir, Tel:+98-912-761-3099

[1]Faculty of Electrical Engineering, Shahid Rajaee Teacher Training University, Lavizan, Tehran, Iran

P.O.Box: 16785-163

Abstract

This paper presents a comprehensive approach for modeling and classification of air gap asymmetry and inter-turn short circuit faults in ladder-secondary linear induction motors (LS-LIMs). It is based on a modified Magnetic Equivalent Circuit (MEC) model incorporated with a current signal-based fault detection method using Convolution Neural Network (CNN). The feature sets of the mentioned faults are classified separately by a CNN, and the training and test data are extracted using three-phase currents obtained from MEC. For this purpose, both healthy and faulty motors are modeled initially by the proposed MEC model to generate different labeled data for training the designed CNNs. It is also shown that fault diagnosis of this motor by Fast Fourier Transform (FFT) is not possible. Finally, the proposed networks are trained based on the obtained currents from Finite Element Method (FEM) to validate their accuracy. Since faults diagnosis in LS-LIMs based on CNN has not been introduced in the relevant literature so far, it is presented in this paper for the first time.

Index Terms

Ladder-secondary linear induction machine (LS-LIM), Inter-turn short circuit, Air gap asymmetry, Magnetic Equivalent Circuit (MEC), Convolution neural network (CNN)

I. INTRODUCTION

Recently, different topologies of linear motors have been modeled and investigated in order to use in various industries. The most common of which are linear synchronous and induction machines (LSMs and LIMs), which are well-known because of their specific features, such as low construction cost and high efficiency, respectively. Although LSMs need a driver to have a stable performance and motion control [1]–[3], LIMs are self starting linear motors with low manufacturing cost and simple structure. Hence, they are widely used in many applications such as rail transportation thanks to their simplicity and low maintenance cost [4], [5]. Traditional LIMs are usually in three-phase type, but they can also be designed based on single and multi-phase power supply [6]. In addition, their secondary structure can be designed in the form of a flat iron sheet [2] or a ladder structure [7]. LIMs inherently suffer from low efficiency and power factor and it is obvious that various faults resulted from electromagnetic and mechanical stress during operation can also cause further reduction in these output parameters. The occurrence of faults disrupts normal operation of motors and even leads to huge economic losses and injury events [8]. Therefore, fault diagnosis can play an active role in increasing the efficiency and lifetime of motors. The basis of any reliable diagnosis method is modeling the motor performance under healthy and faulty conditions, so a comprehensive model of ladder-secondary linear induction motors (LS-LIMS) considering all their phenomena is required [9]. Finite Element Method (FEM) and Magnetic Equivalent Circuit (MEC) have been so far the most popular and effective methods for modeling of electrical machines. However, MEC method has more adjustable accuracy and shorter simulation time in comparison with FEM [10]. A comprehensive MEC model with adjustable accuracy for a healthy LS-LIM considering end-effect and saturation is proposed in [7], which is also used in this paper after some modifications to model both healthy and faulty cases by a single MEC model.

Although there are many researches about different faults diagnosis in rotatory electrical machines in the literature [11]–[15], very limited investigations have been conducted about LIMs fault detection, so far [16]–[20]. The current signature analysis (CSA) and vibration signal analysis are known as the main fault diagnosis methods [21]. However, fault detection based on the stator current is more popular due to the sensitivity of vibration to background noise [22]. Inter-turn short circuit in a LIM is studied and detected in [16], using a parameter evaluation method based on 3-phase equivalent circuit model. In [17], CSA is applied for detection and estimation of bearing faults in induction machines, where Fast Fourier Transform (FFT) is used to determine the severity of an outer race bearing fault. Using vibration signals for bearing fault detection based on FFT in different situations encountered during operation without considering LIMs phenomena is presented in [18]. In [19], an asymmetric structure of MEC is introduced for analysis of the internal short circuit fault in LIMs, where the end effect and saturation are neglected.

In [20], the healthy and faulty LIMs are simulated by time stepping FEM and a Fourier-based transform is applied to analyze the air gap asymmetry fault. The end effect and saturation are not considered accurately in these researches, which can affect fault diagnosis.

Recently, deep learning methods (DL) [23] have also drawn significant attention in electrical machines fault detection thanks to their success in pattern recognition and classification [22], [24]–[27]. The most noticeable advantage of DL methods over classical ones is their strong capability for automatically extracting features from raw data [22]. In [24], diagnosing gear fault in a rotary LIM based on two main modules called information fusion and decision making is presented. Inter-turn short circuit fault in permanent magnet synchronous motor is detected by a DL-based method in [26] to show its higher accuracy compared to classical methods. Convolution Neural Network (CNN) is also one of the most widely used DL-based methods that have multiple layers. A CNN classifier for gearbox faults under various constant loads and speeds is presented in [28]. Based on the authors' knowledge and the above illustrations, it seems that few investigations have been done on fault detection in LS-LIMs. Therefore, this paper presents a comprehensive approach based on a modified MEC model according to [7] incorporated with CNN to detect inter-turn short circuit and air gap asymmetry faults. Therefore, the paper novelties are summarized as follows:

A- Modeling inter-turn and air gap asymmetry faults in a LS-LIM based on a flexible MEC model under different conditions.

B- Diagnosis and classification of inter-turn and air gap asymmetry faults in a LS-LIM by two separate CNNs.

II. Considered MEC for LS-LIM Modeling

In this paper, both healthy and faulty LS-LIMs are modeled by a single MEC model thanks to its capability and shorter processing time compared to FEM. The flexible MEC model is used recently for modeling rotational [29], [30], and linear electric machines modeling [7]. This flexible model is capable of modeling LS-LIM with different dimensions, poles and slot numbers under different loads, where the core nonlinearity is fitted on the material B-H curve. This model also makes it possible to consider end effect that is an important phenomenon in linear motors [31], actuators, and sensors [32], [33] by considering two virtual zones with desired accuracy at both entrance and exit ends of the primary. It is notable to say that current features in a LS-LIM are influenced by end effect in addition to saturation, so considering this can have a significant impact on finding the faults detection patterns. The motor structure and its MEC model are shown in Figs. 1 and 2, respectively. Moreover, the matrix form of the

whole system equations derived from MEC model is written in Eq. (1), where all of the space and time harmonics are considered. All of the equations leading to this general equation are fully explained in [7].

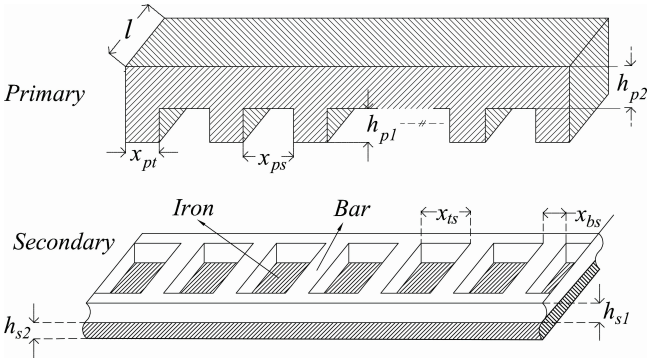

Fig. 1. LS-LIM structure and dimension

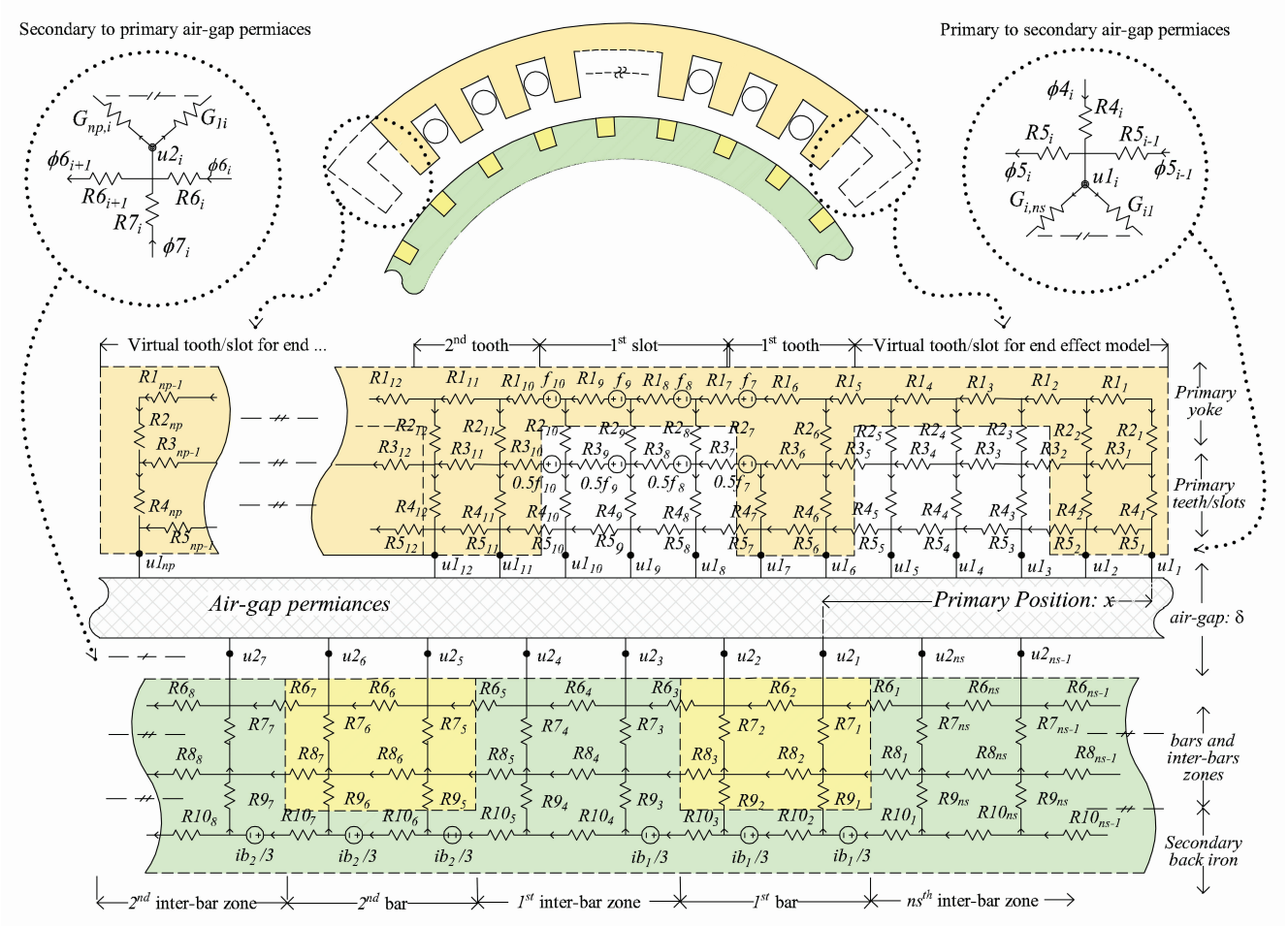

Fig. 2. Proposed MEC for a sample of LS-LIM with $n_v = 1, n1_1 = 2, n1_2 = 3, n2_1 = 2, n2_2 = 2$

$$\begin{cases} \mathbf{A}\Big(\mathbf{X}(t)\Big).\mathbf{X}(t) = \mathbf{B}(t-\Delta t) \\ \mathbf{X}(t) = [\mathbf{\Phi 1}(t) \quad \mathbf{\Phi 3}(t) \quad \mathbf{\Phi 5}(t) \quad \mathbf{\Phi 6}(t) \quad \mathbf{\Phi 8}(t) \quad \mathbf{\Phi 10}(t) \quad \mathbf{Is}(t) \quad \mathbf{Ir}(t) \quad \mathbf{U1}(t) \quad \mathbf{U2}(t)]^T \end{cases} \tag{1a}$$

$$\begin{bmatrix} \mathbf{MpA12} & \mathbf{0.5MpA12} & \mathbf{0} & \mathbf{0} & \mathbf{0} & \mathbf{0} & \frac{\Delta t}{2}\mathbf{R}+\mathbf{L} & \mathbf{0} & \mathbf{0} & \mathbf{0} \\ \mathbf{0} & \mathbf{0} & \mathbf{0} & \mathbf{0} & \mathbf{0} & \mathbf{ApA67} & \mathbf{0} & -\frac{\Delta t}{2}\mathbf{R_{BR}} & \mathbf{0} & \mathbf{0} \\ \mathbf{M1} & \mathbf{-R3} & \mathbf{0} & \mathbf{0} & \mathbf{0} & \mathbf{0} & \mathbf{-0.5Wp} & \mathbf{0} & \mathbf{0} & \mathbf{0} \\ \mathbf{M2} & \mathbf{M3} & \mathbf{-R5} & \mathbf{0} & \mathbf{0} & \mathbf{0} & \mathbf{-0.5Wp} & \mathbf{0} & \mathbf{0} & \mathbf{0} \\ \mathbf{0} & \mathbf{0} & \mathbf{-R5} & \mathbf{0} & \mathbf{0} & \mathbf{0} & \mathbf{0} & \mathbf{Ap} & \mathbf{0} & \mathbf{0} \\ \mathbf{A12} & \mathbf{A12} & \mathbf{A12} & \mathbf{0} & \mathbf{0} & \mathbf{0} & \mathbf{0} & \mathbf{-App} & \mathbf{-Aps} & \mathbf{0} \\ \mathbf{0} & \mathbf{0} & \mathbf{0} & \mathbf{0} & \mathbf{M4} & \mathbf{M5} & \mathbf{0} & \mathbf{0} & \mathbf{0} & \mathbf{-As} \\ \mathbf{0} & \mathbf{0} & \mathbf{0} & \mathbf{0} & \mathbf{-R8} & \mathbf{M6} & \mathbf{0} & \mathbf{AfAbr} & \mathbf{0} & \mathbf{0} \\ \mathbf{0} & \mathbf{0} & \mathbf{0} & \mathbf{-R6} & \mathbf{0} & \mathbf{0} & \mathbf{0} & \mathbf{0} & \mathbf{As} & \mathbf{0} \\ \mathbf{0} & \mathbf{0} & \mathbf{0} & \mathbf{As} & \mathbf{As} & \mathbf{As} & \mathbf{0} & \mathbf{-Asp} & \mathbf{-Ass} & \mathbf{0} \end{bmatrix} \cdot \begin{bmatrix} \mathbf{\Phi 1} \\ \mathbf{\Phi 3} \\ \mathbf{\Phi 5} \\ \mathbf{\Phi 6} \\ \mathbf{\Phi 8} \\ \mathbf{\Phi 10} \\ \mathbf{Is} \\ \mathbf{Ir} \\ \mathbf{U1} \\ \mathbf{U2} \end{bmatrix} = \begin{bmatrix} \mathbf{c1} \\ \mathbf{c2} \\ \mathbf{0} \\ \mathbf{0} \\ \mathbf{0} \\ \mathbf{0} \\ \mathbf{0} \\ \mathbf{0} \\ \mathbf{0} \\ \mathbf{0} \end{bmatrix} \tag{1b}$$

III. Faults Modeling

Studied faults are shown in Fig. 3, where inter-turn fault is modeled by creating a short circuit on phase A. For this purpose, Nf of the total turns (Ns) are shorted by Rf resistance, so $Rf \to \infty$ and $Rf \to 0$ denote healthy and faulty conditions, respectively. Moreover, air gap asymmetry is modeled by defining two different values for the machine air gap at the entrance and exit ends ($\delta 1$ and $\delta 2$). Hence, **Ass**, **App**, **Aps**, **Asp**, **Wp**, **Rs** and **Mp** matrices in [7] need to be changed due to some modifications in the air gap permeances and primary windings resistance and inductance matrices.

A. Air Gap Permeances for Asymmetry Modeling

The air gap permeances are modeled for healthy and faulty LS-LIM with air gap asymmetry. Considering $0 \leq m \leq 1$ as the asymmetry indexes, the permeance between the i^{th} mover and j^{th} stator flux tubes function (G') is computed by Eq. (5) based on Eqs. (2)-(4).

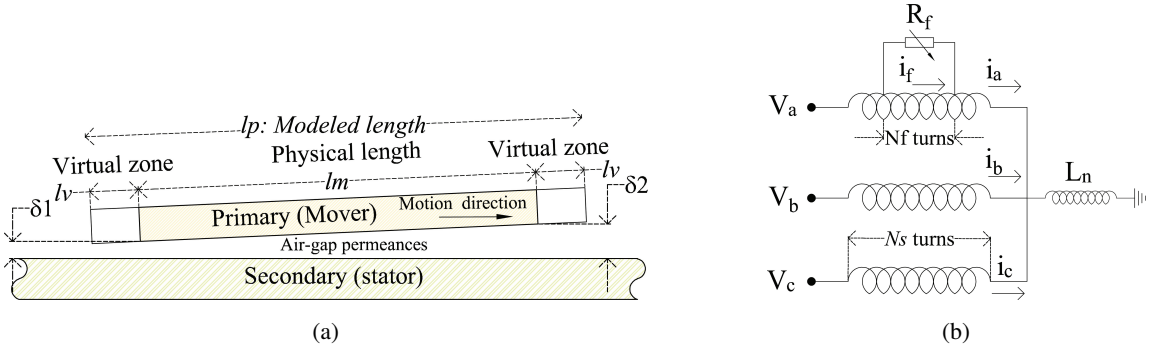

Fig. 3. Studied faults (a)- Air gap asymmetry fault (b)- Windings diagram in healthy and faulty cases with inter-turn fault

$$\vartheta(\theta) = \log\left(\frac{\cosh(\pi\frac{\theta-\gamma_t}{2\beta})\cosh(\pi\frac{\theta+\gamma_t}{2\beta})}{\cosh(\pi\frac{\theta}{2\beta})\cosh(\pi\frac{\gamma}{2\beta})}\right) - \frac{\gamma t^2}{2\beta} \tag{2}$$

$$G(\theta) = \left(\frac{\vartheta(\theta) - \vartheta(\pi)}{\vartheta(0) - \vartheta(\pi)}\right) \tag{3}$$

$$Gp(\theta) = \sum_{k=-1}^{1} G(\theta - 2k\pi) \tag{4}$$

$$G'(\theta_{act}, i, j) = Gp\Big(\theta - (i-1)\gamma p + (j-1)\gamma s\Big) \tag{5}$$

In the Eqs (2)-(5):

$$\begin{cases} \gamma p = \frac{\theta_p}{np}, \gamma s = \frac{2\pi}{ns}, \gamma t = \max(\gamma s, \gamma p) \\ \beta = \log(\frac{r_{pi}}{r_{so}}) \end{cases} \tag{6}$$

G_m is defined as bellow function, where $gap(\theta_{act}, i, m)$ is the air-gap function.

$$G_m(\theta, i, m) = \mu_0 \times l \times \frac{\min(lp/np, ls/ns)}{gap(\theta, i, m)} \tag{7}$$

The permeance between the given i and j nodes (G_{ij}) can be computed by Eq. (8), where the gap function is written in Eq. (9).

$$G_{ij} \triangleq G_m(\theta, i, m)G'(\theta, i, j) \tag{8}$$

$$\begin{cases} gap(\theta, i, m) = \delta_1 + \gamma_m(i-1)m - \frac{lv}{lm}(\delta 2 - \delta 1) \\ m = \frac{\delta 2 - \delta 1}{\theta_p}\frac{lp}{lp+2lv} \end{cases} \tag{9}$$

B. Inter-Turn Fault Modeling

Inter-turn fault modeling needs some modifications in windings resistance and inductance matrices compared to [7]. Considering Nw as the total number of the conductors per phase, the **Rs** and **L** matrices with shorted part in phase A can be written as below:

$$\mathbf{Rs} = \begin{bmatrix} R_a(1-\frac{Nf}{Nw}) + R_f & 0 & 0 & -R_f \\ 0 & R_a & 0 & 0 \\ 0 & 0 & R_a & 0 \\ 0 & 0 & -Rf & Ra(\frac{Nf}{Nw}) + Rf \end{bmatrix} \tag{10}$$

$$\mathbf{L} = \begin{bmatrix} L_n & L_n & L_n & 0 \\ L_n & L_n & L_n & 0 \\ L_n & L_n & L_n & 0 \\ 0 & 0 & 0 & 0 \end{bmatrix} \tag{11}$$

IV. Fault Diagnosis Method

In this section, the fault detection methods are applied to a 2-pole LS-LIM with parameters tabulated in Table I. The studied machine is chosen deliberately because the end effect phenomenon has more vivid influence on the current signature of LS-LIMs with a lower pole pair number (lower than 6) [31]. At first, it is shown that current signature analysis using FFT method is not efficient for fault diagnosis of this machine. Hence, signal analysis based on CNN is used to provide an accurate results. Some procedure of classical fault diagnosis methods can be omitted by using deep learning technique. In spite of classical methods, it can help to find patterns of signals which are not recognizable directly by user [26].

TABLE I

PARAMETERS OF SIMULATED LS-LIM (270 V_{rms}, Y CONNECTED) [7]

Dimension		
Parameter	**Symbol**	**value**
Number of primary slots	n_{ps}	6
Effective depth (cm)	l	15
Primary yoke height (cm)	h_{p2}	2
Primary slot height (cm)	h_{p1}	3
Secondary bar height (cm)	h_{s1}	0.3
Secondary iron height (cm)	h_{s2}	1
Width of the primary slot (cm)	x_{ps}	1
Width of the primary tooth (cm)	x_{pt}	2.5
Virtual zone width (cm)	x_v	5
Mass of the primary (kg)	m	12
Secondary inter-bars width (cm)	x_{ts}	1
Secondary bars width (cm)	x_{bs}	1
Air-gap length (mm)	δ	5
Electrical properties		
Parameter	**Symbol**	**value**
Rated power (kW)	P_{max}	3.5
Rated speed (m/s)	v_m	5.5
Number of poles	p	2
Turn number/pole/ phase	Ns	200
Windings resistance (Ω)	R_a	2
Copper Bars resistivity $(\Omega.m)$	ρ	17×10^{-9}
Voltage source frequency (Hz)	f	50
Synchronous speed (m/s)	v_{syn}	9.5
Considered accuracy		
Parameter	**Symbol**	**value**
Number of flux tubes in x_v	nv	1
Number of elements in x_{ps}	$n12$	3
Number of flux tubes in x_{pt}	$n11$	2
Number of flux tubes in x_{bs}	$n21$	2
Number of flux tubes in x_{ts}	$n22$	2

A. Application of FFT for Fault Diagnosis

Fourier transform is the most common frequency domain tool, which can extract the main point of amplitude, harmonic amplitude and sidebands. This diagnosis algorithm needs two steps of feature extraction and fault classification depending on expert's experience. Classification and finding a proper pattern based on fault signs in this way is very difficult and even impossible, especially in complex machines. Since LS-LIMs current signature is affected by end effect in addition to saturation, its fault

detection is more complicated than rotary ones. In order to investigate the performance of FFT, the LS-LIM under different loads are simulated and some of results are shown in Fig. 4. It is notable to say that the synchronous speed of this motor which is actually the same as the unloaded speed is $v_{syn} = 9.5\ m/s$. The simulated scenarios are as follows:

Scenario 1: Healthy LS-LIM under $F_L = 200\ N$ and $F_L = 400\ N$.

Scenario 2: Asymmetric air gap (ASG) fault with $\delta 1 = 2.5\ mm$ and $\delta 2 = 7.5\ mm$ under $F_L = 200\ N$ and $F_L = 400\ N$.

Scenario 3: Inter-turn short circuit fault (IT) with $Rf = 0.2\ \Omega$ and $N_f = 5$ under $F_L = 200\ N$ and $F_L = 400\ N$.

Based on the authors' investigations, finding any patterns related to slip and speed according to the obtained harmonic spectrums for this machine is not possible due to its complexity. Therefore, a CNN framework based on deep learning method is needed, which its usage in machine fault diagnosis is a relatively new area. CNN has the ability of automatic feature extraction, and this makes it resilient to dependence on manual feature extraction and selection.

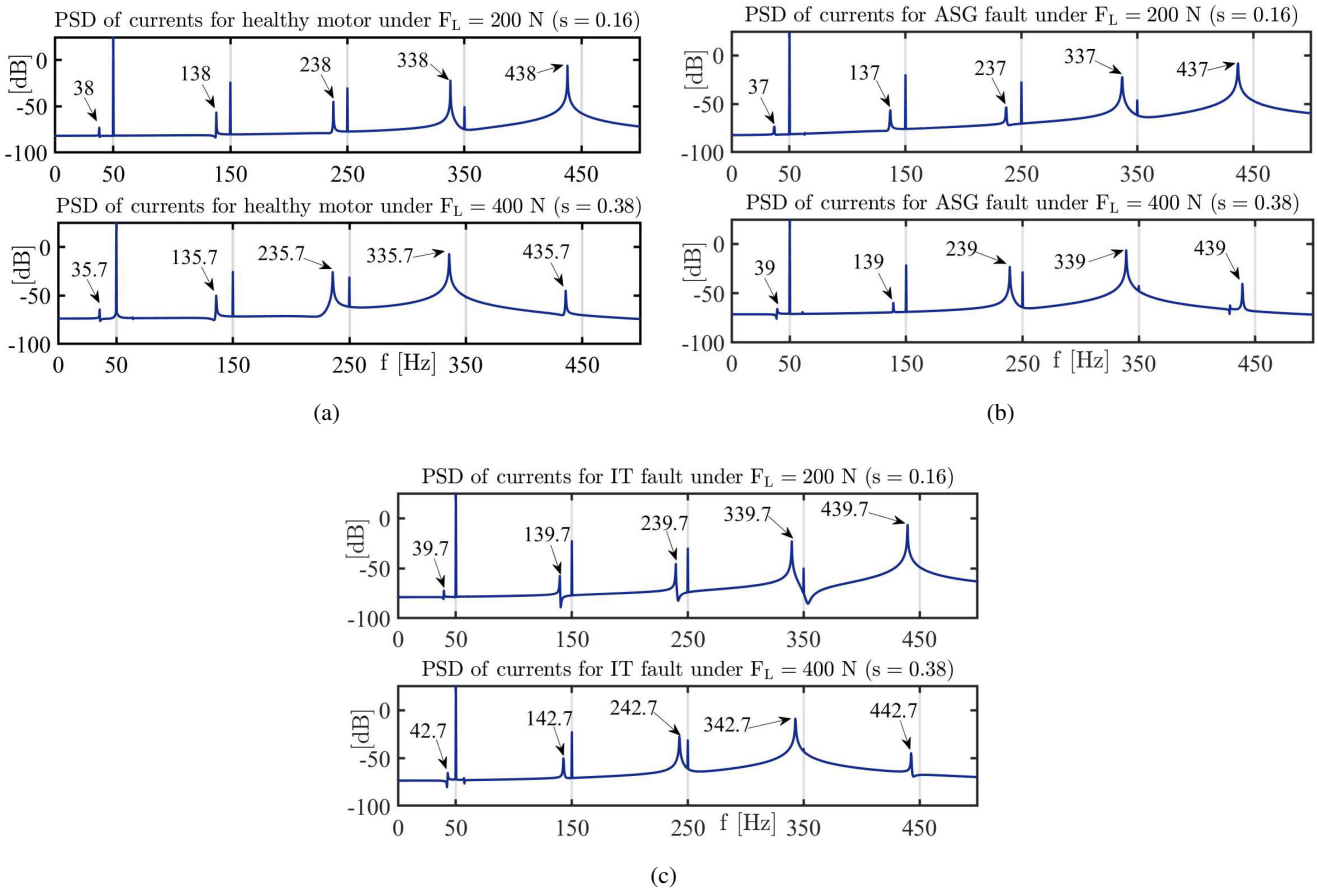

Fig. 4. PSD of stators' current under healthy and faulty conditions (a)- healthy (b)- ASG fault (c)-IT fault

B. Application of CNN for Fault Diagnosis

Data-driven fault classifiers such as CNN method have sparked great interests in fault diagnosis of electrical machines. It is one of the most effective DL-based network for signal classification, especially where the significant features are ambiguous. In fact, resorting to a proper set of input features is the most significant advantage of neural network methods over traditional techniques [34]. The schematic of a typical CNN is shown in Fig. 5, where its several layers jointly perform both feature extraction and classification functions. As can be seen, it consists of an input layer, an output layer, and multiple hidden layers (a series of convolutional layers). At first, raw data for both healthy and faulty conditions resulted from modeling are fed to the network by input layer. Then, various features are learnt from the training data in convolutional layers (CONV). They are sometimes followed by activation functions, pooling, normalization, or fully connected layers. Finally, the extracted features are fed into a fully connected layers with the Softmax activation function to drive the final classification decision.

V. Simulation Results

In this section, simulation results for healthy and faulty cases are presented to evaluate the effectiveness of the proposed method. For this purpose, the performance of LS-LIM under healthy and faulty conditions including inter-turn, air gap asymmetry and both faults simultaneously are simulated to train and test the CNNs. In the proposed fault detection method, two networks are designed for diagnosing each studied fault because their extracted features are so close to each other, which makes it impossible to use a single CNN. However, the measured winding currents are the input of both CNNs and the architectures of them are the same. The mentioned CNNs consist of different layers as follows:

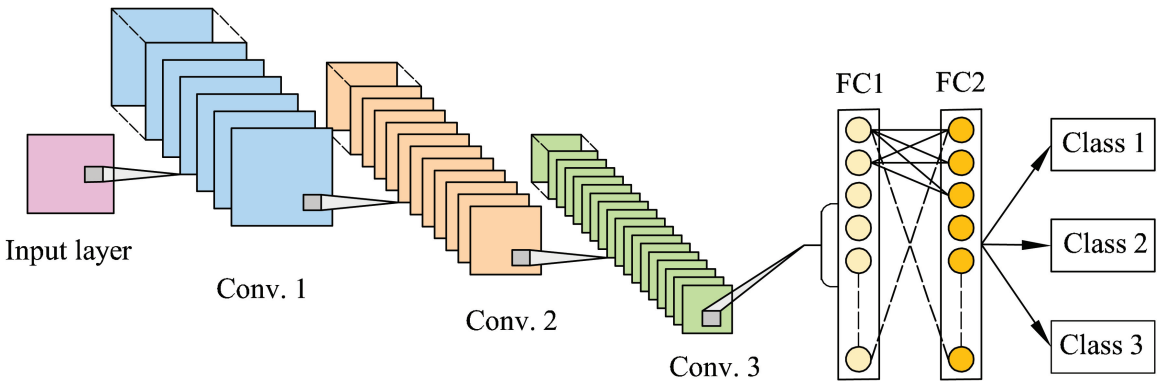

Fig. 5. A sample schema of a CNN with three hidden layers

⊛-A 2D input layer

⊛-A CONV layer with five 3×5 filters and hyperbolic tangent activation function

⊛-A max pooling layer to reduce dimension of the features without losing information

⊛-A CONV layer with fifteen 3×5 filters and rectified linear unit activation function

⊛-Another max pooling layer to reduce the number of parameters and computation in the network

⊛-A dropout layer

⊛-A FC with 2 neurons and Softmax activation function corresponding to motor operation conditions as the output layer

The batch size and learning rate of CNNs are heuristically adjusted at 64 and 0.005, respectively. The simulation results are separated into train and test datasets, while 20% of the training data is randomly selected for validation. The obtained currents from simulation of the mentioned scenarios in Table II are used to provide train and test datasets, where the duration and sampling time for each scenario is 1.5 sec and 0.5 msec, respectively. It is notable that a window with a length of 200 samples is also applied on the measured signals, so a 3×200 matrix yields as the input layer of the CNNs. The last half second of the measured signals are used for training and testing procedures in which the overlap of two consecutive windows is 50 samples. Since the training procedure is a stochastic one, its algorithm is repeated 20 times for each CNN to reach reliable results.

According to the presented mean and standard deviation in Table III, it can be seen that the accuracy of both networks for training and testing data are more than 90%. The confusion matrices for both proposed CNNs are also brought in Table IV to show the accuracy of each network in classification of different cases. It is illustrated that the proposed CNN for detection of inter-turn fault can predict the whole faulty cases accurately and only 7% of healthy cases are misclassified. On the other hand, another CNN can classify all healthy cases correctly and its prediction accuracy for distinguishing air gap asymmetry fault is 90%. Therefore, the proposed method provides an intelligent, efficient, and computationally viable solution for the multiple fault diagnosis in LS-LIM compared to FFT. It is notable to say that this method is faster than FFT because after giving the resulted currents to these networks, they can predict the related classes automatically and do not depend on the user's decision.

TABLE II

DIFFERENT CONSIDERED SCENARIOS FOR GENERATION TRAIN AND TEST DATASETS

Data	Condition	F_L (N)	Nf	R_f (Ω)	$\delta 1$ (mm)	$\delta 2$ (mm)
Train	Healthy	0	0	∞	5	5
		200	0	∞	5	5
	ASG	250	0	∞	7	3
		250	0	∞	8	2
		350	0	∞	4	6
		450	0	∞	7.5	2.5
	IT	0	10	1	5	5
		200	5	0.05	5	5
		200	5	1	5	5
		400	5	1	5	5
		400	5	10	5	5
		600	5	10	5	5
	IT & ASG	0	5	0.05	4	6
		200	5	0.05	4	6
Test	Healthy	400	0	∞	5	5
	ASG	250	0	∞	6	4
		300	0	∞	4.5	5.5
	IT	150	30	0.25	5	5
		200	40	1	5	5
		250	100	5	5	5
		300	5	0.05	5	5
		400	5	0.05	5	5
	IT & ASG	300	5	0.05	4	6
		400	5	0.05	4	6

TABLE III

MEAN AND STANDARD DEVIATION OF ACCURACY FOR DESIGNED CNNS

	Accuracy	
	Train Dataset	**Test Dataset**
CNN for IT Fault Detection	$96 \pm 2\%$	$93 \pm 3\%$
CNN for ASG Fault Detection	$98 \pm 1\%$	$92 \pm 2\%$

TABLE IV
CONFUSION MATRICES FOR DESIGNED CNNS

CNN for IT fault diagnosis	Predicted Class	
	Healthy	IT
Healthy	0.93	0.07
IT	0	1.00
CNN for ASG fault diagnosis	Predicted Class	
	Healthy	ASG
Healthy	1.00	0
ASG	0.10	0.90

VI. VALIDATION BY 2D FEM

In this part, the designed CNNs are trained by the obtained currents from 2D-FEM via Maxwell software based on the same assumptions as mentioned in the section V and defined parameters in Table I. A 16 MB-RAM, 2.5 GHz computer is used for simulation, where a 0.01 mm Length-based Mesh and $\Delta t = 0.005$ ms are applied to reach trustable results. For this purpose, several healthy and faulty scenarios are simulated by 2D-FEM as below:

Scenario 1: No-load Healthy LS-LIM.
Scenario 2: Healthy LS-LIM under $F_L = 200\ N$.
Scenario 3: LS-LIM with ASG fault ($\delta 1 = 2.5\ mm$ and $\delta 2 = 7.5\ mm$ under $F_L = 250\ N$).
Scenario 4: LS-LIM with ASG fault ($\delta 1 = 4\ mm$ and $\delta 2 = 6\ mm$ under $F_L = 200\ N$).
Scenario 5: LS-LIM with IT fault ($Rf = 0.5\ \Omega$ and $N_f = 10$ under $F_L = 200\ N$).
Scenario 6: LS-LIM with IT fault ($Rf = 10\ \Omega$ and $N_f = 10$ under $F_L = 400\ N$).

The resulted currents are given to the proposed CNNs, and the accuracy of test datasets for the neural networks are shown in Table V. As can be seen, the accuracy of the proposed CNNs for the whole test datasets are more than 90% based on the obtained currents from 2D FEM. It can be concluded that the fault diagnosis networks based on FEM results have a good accuracy as well as based on the obtained currents from MEC. Moreover, some of the resulted currents curves from FEM are illustrated in Fig. 6 to show that faulty cases are not possible to be detected by comparing the general form of currents figures in faulty machine with the healthy one without extraction of their frequency features and finding a proper pattern.

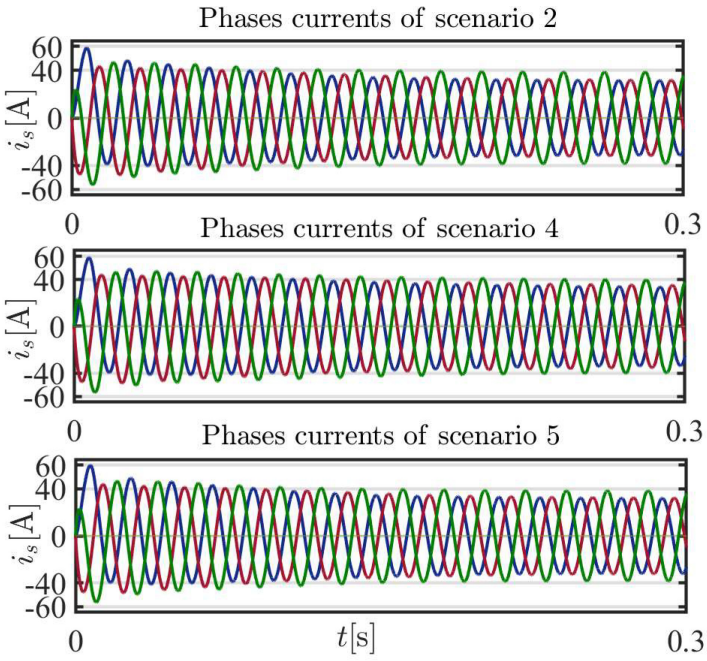

Fig. 6. Currents curves for some investigated scenarios

Moreover, in Fig. 7 figure, it is shown that there is a minor difference between the current amplitude of phase A in faulty scenarios in comparison with the healthy one. In addition, thrust and primary speed of machine for these scenarios are brought in Fig. 8. As can be seen from these figures, it is impossible to diagnose faulty cases from speed, current or thrust curves with the naked eye and it requires a comprehensive approach.

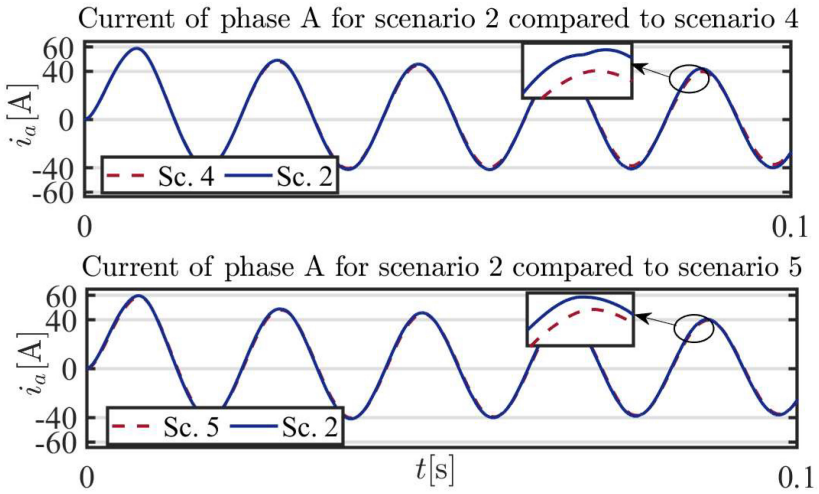

Fig. 7. Thrust and primary speed for some scenarios

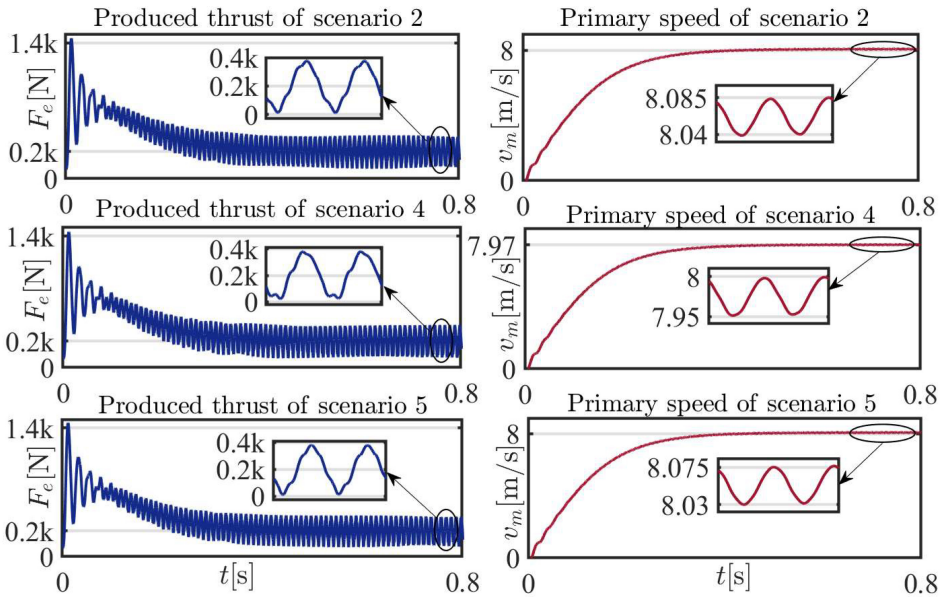

Fig. 8. Thrust and primary speed for some scenarios

TABLE V

ACCURACY OF THE DESIGNED CNNS BASED ON FEM RESULTS

Scenario	Test Dataset
Healthy (1)	95%
Healthy (2)	91%
ASG (3)	90%
ASG (4)	92%
IT (5)	93%
IT (6)	93%

VII. CONCLUSION

In this paper, a novel method for multiple faults classification in a 2-pole LS-LIM using a convolutional neural network based on a comprehensive MEC model is presented. It is demonstrated that, despite the fact that CNN algorithms require a large dataset to train, they can automatically perform adaptive feature extractions on the obtained currents without any prior expertise on fault characteristic frequencies. This feature makes this method more efficient than FFT in finding a proper pattern in a such complicated machine, which is impossible or very difficult to be derived by user directly. Moreover, the confusion matrices for the designed CNNs show that they have an acceptable accuracy in classifying air gap asymmetry and inter-turn short circuit faults. For validation, the obtained currents from 2D FEM in both faulty and healthy conditions are also given to the designed CNNs, which confirm the good accuracy of the proposed networks.

REFERENCES

[1] Salimi, H., Zakipour, A., and Asadi, M. "A novel analytical approach for time-response shaping of the pi controller in field oriented control of the permanent magnet synchronous motors," *Journal of Electrical and Computer Engineering Innovations (JECEI)*, pp. 463–476, 2022.

[2] Niknafs, S., Shiri, A., and Bagheri, S. "Modeling and analysis of flat double-sided linear permanent magnet synchronous generator by magnetic equivalent circuit," *Journal of Electrical and Computer Engineering Innovations (JECEI)*, vol. 10, no. 1, pp. 17–24, 2022.

[3] Heidary, M., Naderi, P. and Shiri, A. "Modeling and analysis of a multi-segmented linear permanent-magnet synchronous machine using a parametric magnetic equivalent circuit," *Electrical Engineering*, vol. 104, no. 2, pp. 705–715, 2022.

[4] Lv, G., Zhou, T., Zeng, D., et al. "Influence of secondary constructions on transverse forces of linear induction motors in curve rails for urban rail transit," *IEEE Transactions on Industrial Electronics*, vol. 66, no. 6, pp. 4231–4239, 2018.

[5] Esfahanian, H. R., Hasanzadeh, S., Heydari, M., et al. "Design, optimization, and control of a linear tubular machine integrated with levitation and guidance for maglev applications," *Scientia Iranica*, 2021.

[6] Hamedani, P., Sadr, S., and Shoulaei, A. "Independent fuzzy logic control of two five-phase linear induction motors supplied from a single voltage source inverter," *Journal of Electrical and Computer Engineering Innovations (JECEI)*, vol. 10, no. 1, pp. 195–208, 2022.

[7] Naderi, P., Heidary, M., and Vahedi, M. "Performance analysis of ladder-secondary-linear induction motor with two different secondary types using magnetic equivalent circuit," *ISA transactions*, 2020.

[8] Faiz, J., Ebrahimi, B., and Sharifian, M. "Different faults and their diagnosis techniques in three-phase squirrel-cage induction motorsa review," *Electromagnetics*, vol. 26, no. 7, pp. 543–569, 2006.

[9] Feng, Z., Chen, X., and Zuo, M. J. "Induction motor stator current am-fm model and demodulation analysis for planetary gearbox fault diagnosis," *IEEE Transactions on Industrial Informatics*, vol. 15, no. 4, pp. 2386–2394, 2018.

[10] Sheikh-Ghalavand, B., Vaez-Zadeh, S., and Isfahani, A. H. "An improved magnetic equivalent circuit model for iron-core linear permanent-magnet synchronous motors," *IEEE Transactions on Magnetics*, vol. 46, no. 1, pp. 112–120, 2009.

[11] Naderi, P. and Shiri, A. "Rotor/stator inter-turn short circuit fault detection for saturable wound-rotor induction machine by modified magnetic equivalent circuit approach," *IEEE Transactions on Magnetics*, vol. 53, no. 7, pp. 1–13, 2017.

[12] Ali, M. Z., Shabbir, M. N. S. K., Liang, X., et al. "Machine learning-based fault diagnosis for single-and multi-faults in induction motors using measured stator currents and vibration signals," *IEEE Transactions on Industry Applications*, vol. 55, no. 3, pp. 2378–2391, 2019.

[13] Corral-Hernandez, J. A. and Antonino-Daviu, J. A. "Thorough validation of a rotor fault diagnosis methodology in laboratory and field soft-started induction motors," *Chinese Journal of Electrical Engineering*, vol. 4, no. 3, pp. 66–72, 2018.

[14] Liang, X., Ali, M. Z., and Zhang, H. "Induction motors fault diagnosis using finite element method: A review," *IEEE Transactions on Industry Applications*, vol. 56, no. 2, pp. 1205–1217, 2019.

[15] Faiz, J., Ghasemi-Bijan, M., and Ebrahimi, B. M. "Modeling and diagnosing eccentricity fault using three-dimensional magnetic equivalent circuit model of three-phase squirrel-cage induction motor," *Electric Power Components and Systems*, vol. 43, no. 11, pp. 1246–1256, 2015.

[16] Utsumi, T. and Yamaguchi, I. "Detection and location of inter-turn short circuit in linear induction motor," in *4th IEEE International Symposium on Diagnostics for Electric Machines, Power Electronics and Drives, 2003. SDEMPED 2003.*, pp. 63–68, IEEE, 2003.

[17] Haddad, R. Z., Lopez, C. A., Pons-Llinares, J., et al. "Outer race bearing fault detection in induction machines using stator current signals," in *2015 IEEE 13th International Conference on Industrial Informatics (INDIN)*, pp. 801–808, IEEE, 2015.

[18] Bianchini, C., Immovilli, F., Cocconcelli, M., et al. "Fault detection of linear bearings in brushless ac linear motors by vibration analysis," *IEEE Transactions on Industrial Electronics*, vol. 58, no. 5, pp. 1684–1694, 2010.

[19] Nosrati, A. and Nazarzadeh, J. "Analysis of linear induction machines with internal fault by mec," *COMPEL-The international journal for computation and mathematics in electrical and electronic engineering*, 2017.

[20] Faiz, J., Ghods, M., and Tajdyni, A. "Dynamic air gap asymmetry fault detection in single-sided linear induction motors," *IET Electric Power Applications*, vol. 14, no. 4, pp. 605–613, 2019.

[21] Chernyavska, I. and Vítek, O. "Analysis of air-gap eccentricity in inverter fed induction motor by means of motor current signature analysis and stray flux of motor," in *2017 IEEE 11th International Symposium on Diagnostics for Electrical Machines, Power Electronics and Drives (SDEMPED)*, pp. 72–76, IEEE, 2017.

[22] Zhang, S., Wang, B., and Habetler, T. G. "Deep learning algorithms for bearing fault diagnostics-a review," in *2019 IEEE 12th International Symposium on Diagnostics for Electrical Machines, Power Electronics and Drives (SDEMPED)*, pp. 257–263, IEEE, 2019.

[23] Topaloglu, I., "Deep learning based convolutional neural network structured new image classification approach for eye disease identification," *Scientia Iranica*, 2022.

[24] Razavi-Far, R., Hallaji, E., Farajzadeh-Zanjani, M., et al. "Information fusion and semi-supervised deep learning scheme for diagnosing gear faults in induction machine systems," *IEEE Transactions on Industrial Electronics*, vol. 66, no. 8, pp. 6331–6342, 2018.

[25] Wang, S., Bao, J., Li, S., et al. "Research on interturn short circuit fault identification method of pmsm based on deep learning," in *2019 22nd International Conference on Electrical Machines and Systems (ICEMS)*, pp. 1–4, IEEE, 2019.

[26] Han, J.-H., Choi, D.-J., Park, S.-U., et al. "A study on fault classification system based on deep learning algorithm considering speed and load condition," in *2019 22nd International Conference on Electrical Machines and Systems (ICEMS)*, pp. 1–4, IEEE, 2019.

[27] Zhang, W., Hu, Y., Zeng, D., et al. "Motor bearing fault diagnosis based on deep learning," in *2019 20th IEEE/ACIS International Conference on Software Engineering, Artificial Intelligence, Networking and Parallel/Distributed Computing (SNPD)*, pp. 8–14, IEEE, 2019.

[28] Chen, Z., Li, C., and Sanchez, R.-V. "Gearbox fault identification and classification with convolutional neural networks," *Shock and Vibration*, vol. 2015, 2015.

[29] Rostami, M., Naderi, P., and Shiri, A. "Modelling and analysis of permanent magnet vernier machine using flexible magnetic equivalent circuit method," *IET Science, Measurement & Technology*, vol. 16, no. 3, pp. 160–170, 2022.

[30] Sharouni, S., Naderi, P., Hedayati, M., et al. "Performance analysis of a novel outer rotor flux-switching permanent magnet machine as motor/generator for vehicular and aircraft applications," *IET Electric Power Applications*, vol. 15, no. 2, pp. 243–254, 2021.

[31] Shiri, A. and Shoulaie, A. "Design optimization and analysis of single-sided linear induction motor, considering all phenomena," *IEEE Transactions on energy conversion*, vol. 27, no. 2, pp. 516–525, 2012.

[32] Paymozd, A., Saneie, H., and Nasiri-Gheidari, Z. "Analytical modelling of linear resolver considering longitudinal end effect," *Scientific Journal of Applied Electromagnetics*, vol. 10, no. 1, 2022.

[33] Zare, F. and Nasiri-Gheidari, Z. "Improving the performance of helical motion resolver based on accurate modelling of longitudinal end effect," *IET Electric Power Applications*, 2022.

[34] Pal, M. and Edwards, M. G. "Archives of computational methods in engineering: Numerical convergence and the maximum principle," *Archives of computational methods in engineering: state of the art reviews*, vol. 17, no. 2, pp. 137–189, 2010.

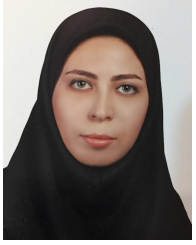

Malihe Heidary was born in Tehran, Iran, in 1989. She received B.Sc. and M.Sc. degrees in electrical engineering from Shahid Beheshti and Olom Tahghighat university of science and technology, Tehran, Iran , in 2013 and 2015, respectively. She is currently working toward the Ph.D. degree in electrical engineering at Shahid Rajaee University of Science and Technology, Tehran, Iran. Her areas of research interests include linear electric machines, renewable energy and design, optimization, and performance analysis of electrical machines.

Vahab Nekoukar received the B.Sc., M.Sc. and Ph.D. degrees in electrical engineering from the Khaje Nasir Toosi University in 2005, Tarbiat Modares University in 2007 and Iran University of Science and Technology in 2012, respectively. In 2014, he joined the School of Electrical Engineering, Shahid Rajaee Teacher Training University, as an assistant professor. His current research interests include control of biological systems, robotics and machine learning.

Peyman Naderi was born in Ahvaz, Iran, in 1975. He received his B.S. degree in Electronic Engineering in 1998 and M.S. degree in Power Engineering from Chamran University, Iran, Ahvaz in 2001. He has a Ph.D. degree in Power Engineering Science from K.N. Toosi University, Tehran, Iran. His interests are electrical machine modeling and fault diagnosis and also power system transient. He is currently associate professor in Shahid Rajaee Teacher Training University of Tehran, Iran.

Abbas Shiri was born in Hashtrood, Iran in 1980. He received the B.Sc. degree from Tabriz University and M.Sc. and Ph.D. degrees from Iran University of Science and Technology all in electrical engineering in 2004, 2006 and 2013, respectively. He is currently an assistant professor at Shahid Rajaee Teacher Training University, Tehran, Iran. His areas of research interests include linear electric machines, electromagnetic systems and actuators, electrical machine design and modeling.